Open Access

Research Article

PRNANO

Precis. Nanomed. 2025, 8(4):1600-1610

ANDOVER HOUSE

GIMAP and Lipid Metabolism Imaging in Clear Cell Renal Cell Carcinoma: A Negative Radiogenomic Analysis

Federico Greco[1,2,3], Marco Cataldo[4], Andrea Panunzio[5], Alessandro Tafuri[5,6], Bruno Beomonte Zobel[3,7], Carlo Augusto Mallio[3,7]

[1]*Ultrasound Radiogenomics AI Center, Via Taranto, 67b, 72026 San Pancrazio Salentino (BR), Italy.*
[2]*Department of Radiology, Cittadella della Salute, Azienda Sanitaria Locale di Lecce, Piazza Filippo Bottazzi, 2, 73100 Lecce, Italy.*
[3]*Research Unit of Radiology, Department of Medicine and Surgery, Università Campus Bio-Medico di Roma, Via Alvaro del Portillo, 21, 00128 Roma, Italy.*
[4]*Apphia srl, via per Monteroni, 73100 Lecce, Italy.*
[5]*Department of Urology, "Vito Fazzi" Hospital, Piazza Filippo Muratore, 1, 73100 Lecce, Italy*
[6]*Tafuri Medical Center, Via A. Gidiuli 36a, 73100 Lecce, Italy.*
[7] *Fondazione Policlinico Universitario Campus Bio-Medico, Via Alvaro del Portillo, 200, 00128 Roma, Italy.*

Submitted: October 12, 2025 Accepted: October 28, 2025 Published: November 2, 2025

Graphical Abstract

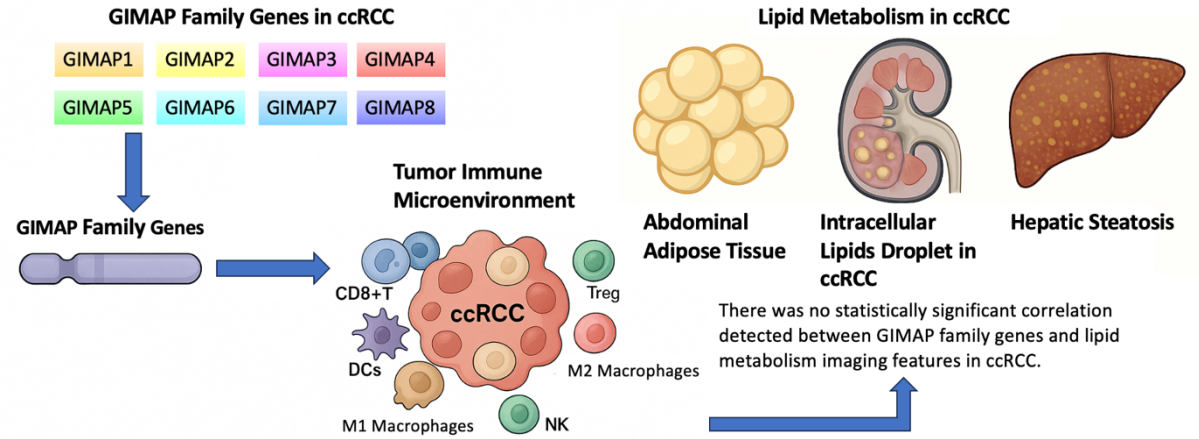

Abstract

Radiogenomics and lipid metabolism are complementary aspects in studying clear cell renal cell carcinoma (ccRCC). The GTPase of immunity-associated proteins (GIMAP) gene family, known for its role in lymphocyte survival and immune regulation, has recently been linked to specific radiogenomic features. This study aimed to determine whether GIMAP expression correlates with radiological markers of lipid metabolism, such as tumor and liver attenuation on non-contrast computed tomography (CT) and abdominal fat distribution. Genomic and imaging data from The Cancer Genome Atlas (TCGA) and The Cancer Imaging Archive (TCIA) were analyzed in a cohort of 205 ccRCC patients. Both traditional and AI-assisted statistical methods (Welch's t-test with FDR-BH correction, equivalence testing, and robust winsorization) showed no significant differences between GIMAP-positive and GIMAP-negative tumors. Average tumor attenuation was similar (36.6 vs. 34.6 HU, p=0.180), as were total, visceral, and subcutaneous fat areas (all p>0.13), along with liver attenuation measures (all p>0.5). These results suggest no meaningful link between GIMAP expression and CT-based lipid metabolism indicators, supporting the idea that GIMAP mainly reflects immune rather than metabolic aspects of tumor biology. CT lipid markers are unlikely to be reliable indicators of GIMAP expression. Future radiogenomic models should incorporate both immune and metabolic factors to improve patient classification in ccRCC.

Keywords: adipose tissue, clear cell renal cell carcinoma, computed tomography, genes, GIMAP, imaging, immunocytes, lipid metabolism, precision medicine, radiogenomics

Purpose, Rationale, and Limitations

The purpose of this study was to explore whether the expression of the GTPase of immunity-associated proteins (GIMAP) gene family correlates with imaging features of lipid metabolism in clear cell renal cell carcinoma (ccRCC). The rationale derives from the recognized involvement of GIMAPs in immune regulation and lymphocyte survival, suggesting a potential interplay between immune signaling and metabolic remodeling within the tumor microenvironment. By analyzing CT-based indicators of lipid accumulation — such as tumor and hepatic attenuation and adipose tissue distribution — this study aimed to determine whether GIMAP expression could be reflected in measurable radiological phenotypes. However, several limitations must be acknowledged: the retrospective design and the use of publicly available The Cancer Genome Archive (TCGA)/The Cancer Imaging Archive (TCIA) datasets may introduce heterogeneity in imaging protocols; Hounsfield Units (HU)-based and single slice adiposity measurements provide indirect, simplified estimates of lipid metabolism; and the absence of direct immune microenvironment markers limits biological interpretation. Future multicenter prospective studies integrating immune and metabolic radiogenomic axes are warranted to validate and expand these findings.

Introduction

Radiogenomics is an interdisciplinary field that studies the relationship between radiological imaging features and the genetic or molecular profiles of tissues. Its goal is to use imaging data to predict gene expression, genetic mutations, or treatment response without always relying on invasive biopsies. It can also be applied in association with lipid metabolism to investigate the links between tumor gene expression, the estimated intracellular lipid content of tumor cells, adipose tissue amount, and hepatic steatosis. By combining radiology and genomics, radiogenomics enables more personalized medicine**,** improving diagnosis, prognosis, and therapy selection [1-5].

The tumor immune microenvironment (TIME) is closely linked to immunotherapy response and clinical outcomes in cancer patients [6–8]. Understanding the main determinants of the TIME is therefore essential for predicting immunotherapy effectiveness and for identifying novel therapeutic targets in ccRCC.

The GIMAP gene family, located on chromosome 7 spanning roughly 500 KB, comprises seven functional members (GIMAP1, GIMAP2, GIMAP4, GIMAP5, GIMAP6, GIMAP7, GIMAP8) and one pseudogene [9]. These proteins share a conserved N-terminal region and contain a guanine nucleotide–binding GTPase domain [9,10]. Most GIMAPs play a role in lymphocyte development and survival [11–15].

Recent evidence indicates that GIMAP family gene expression in ccRCC is associated with distinct CT radiogenomic features. In a retrospective cohort, GIMAP-positive tumors were more frequently observed in older patients. They were correlated with high Fuhrman grade, absence of endophytic growth, and imaging signs of tumor infiltration [1]. These findings suggest that radiogenomics may provide non-invasive markers of GIMAP expression, offering potential insights into tumor aggressiveness and therapeutic stratification.

In obesity, adipose tissue develops chronic inflammation, with an increase in pro-inflammatory immune cells (CD8+, Th1, B2) and a reduction in regulatory ones (Treg, Th2), contributing to the development of insulin resistance and type 2 diabetes [16].

It is now recognized that excess adipose tissue, particularly visceral adipose tissue (VAT), plays an active role in the development of renal cell carcinoma (RCC). In fact, higher VAT volumes have been reported in patients with ccRCC [3,4]. When adipocytes undergo reduced oxygen availability, hypoxia-inducible factor 1 (HIF-1) is released from the expanded adipose depots, together with altered secretion of adipokines such as leptin, adiponectin, resistin, and visfatin. This dysregulated signaling may provide a mechanistic link between obesity and RCC initiation [17–19].

Hypothesis

This study hypothesizes that GIMAP gene family expression is associated with imaging features of lipid metabolism in ccRCC. Considering the pivotal role of GIMAPs in regulating lymphocyte function and survival, along with the immunomodulatory activity of VAT in chronic inflammation and metabolic stress, a functional connection between tumor immune

regulation, lipid metabolism, and GIMAP expression is biologically plausible. Therefore, this study investigates whether specific imaging markers of lipid metabolism, including intracellular lipid accumulation, adipose tissue distribution, and hepatic steatosis, are associated with GIMAP expression profiles in ccRCC. This integrated radiogenomic and metabolic approach seeks to provide novel insights into the biological mechanisms of ccRCC and to identify potential non-invasive biomarkers for improved patient stratification.

Materials and Methods

The Cancer Genome Atlas

TCGA, a project supported by the National Cancer Institute and the National Human Genome Research Institute (NHGRI), has assembled a comprehensive catalog of genomic alterations across more than 20 cancer types, including ccRCC. Tissue specimens provided by participating centers, following institutional review board approval, underwent extensive multi-platform genomic profiling and evaluation. Imaging data, collected before treatment, were uploaded to TCIA, an anonymized image repository funded by the National Cancer Institute, in DICOM format. Each imaging record is cross-referenced with the corresponding TCGA tissue sample using a unique identifier, and the data are publicly available for download [20].

Imaging Features of Lipid Metabolism

In evaluating imaging markers of lipid metabolism in ccRCC, both tumor and hepatic attenuation values in HU and the distribution of abdominal fat compartments were systematically analyzed. For renal tumors, attenuation was determined on non-contrast CT scans by placing a region of interest (ROI) over the solid area of the tumor while avoiding visible necrosis, cystic degeneration, calcifications, or adjacent non-tumor tissues, from which minimum, maximum, and average HU values were extracted [3-5]. Representative CT images showing ROI placement on the tumor and hepatic parenchyma are provided in Figure 1. For the liver, ROIs were positioned in homogeneous parenchymal regions, carefully avoiding vascular structures, biliary ducts, and beam-hardening artifacts, recording the corresponding minimum, maximum, and average HU values [5]. To verify measurement reliability, a secondary ROI corresponding to 5% of the primary ROI area was randomly positioned within the same anatomical region and used to confirm consistency between primary and secondary attenuation values.

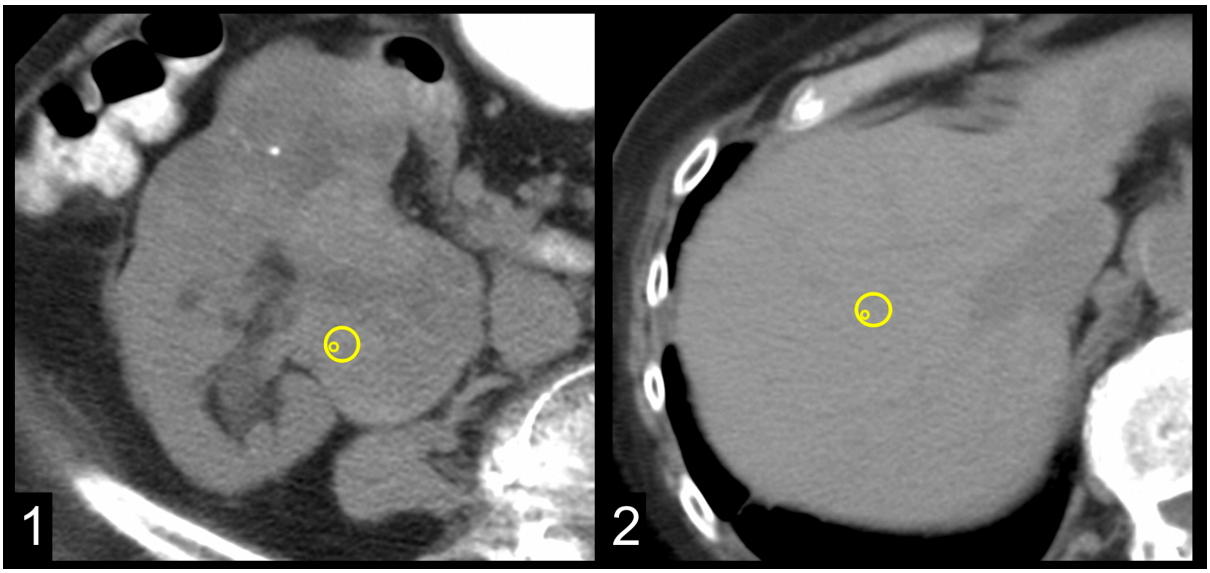

Figure 1. *Representative CT images showing region of interest (ROI) placement for attenuation measurements. (1) Axial unenhanced CT image of a ccRCC. The yellow circle indicates the ROI positioned over the solid portion of the tumor, carefully avoiding areas of necrosis, cystic degeneration, calcifications, or adjacent non-tumor tissues. The smaller concentric circle indicates the secondary ROI (5% of the primary area) and serves as an internal consistency check for measurement reproducibility. (2) Axial unenhanced CT image of the liver, with the ROI placed within homogeneous parenchyma, avoiding vascular structures, biliary ducts, and beam-hardening artifacts. The smaller concentric ROI (5%) was used for internal validation. These examples illustrate the standard procedure used for ROI placement in tumor and hepatic attenuation analysis.*

If the difference between the two exceeded 5 HU, measurements were repeated. This procedure provided an internal check to ensure reproducibility and to reduce operator-dependent bias. The relationship between HU values and intracellular lipid content derives from the physical properties of X-ray attenuation. Lipids, having lower density and atomic number than water and proteins, attenuate X-rays less efficiently, resulting in lower CT attenuation values. Therefore, a decrease in HU within solid tissue regions indicates a higher lipid fraction within cells. This inverse correlation has been consistently demonstrated in previous radiogenomic studies of ccRCC, where reduced unenhanced CT attenuation corresponds to increased lipid storage at the cellular level [4,5]. This method provides an indirect estimate of intracellular lipid content. Given that adipose tissue typically ranges between −50 and −100 HU, lower attenuation in solid tumor and hepatic regions is indicative of greater lipid accumulation in cells [4,5]. All ROIs were manually delineated by two board-certified radiologists (with 9 and 13 years of experience, respectively), both of whom were blinded to clinical and molecular data. Discrepancies were resolved by consensus. Quantification of abdominal fat compartments, including total adipose tissue (TAT), VAT, and subcutaneous adipose tissue (SAT), was performed using a semi-automated function available in Horos software version 4.0.0 RC2 [3-5]. The software automatically detected pixels within the predefined HU range, while manual refinement was applied along the abdominal muscular fascia to accurately separate visceral from subcutaneous compartments. Each measurement was independently verified by two experienced radiologists, blinded to clinical and genomic data. Intra- and inter-observer reproducibility was tested in a random subset (20%) of cases, yielding intraclass correlation coefficients (ICC) of 0.95 for VAT, 0.93 for SAT, and 0.96 for TAT, indicating excellent agreement. Segmentations with >5% discrepancy between observers were re-evaluated by consensus.

This semi-automated, threshold-based workflow ensured high reproducibility and standardization across the dataset. Representative axial CT images illustrating the segmentation of TAT, VAT, and SAT, together with comparative examples of GIMAP-positive and GIMAP-negative cases, are shown in Figure 2.

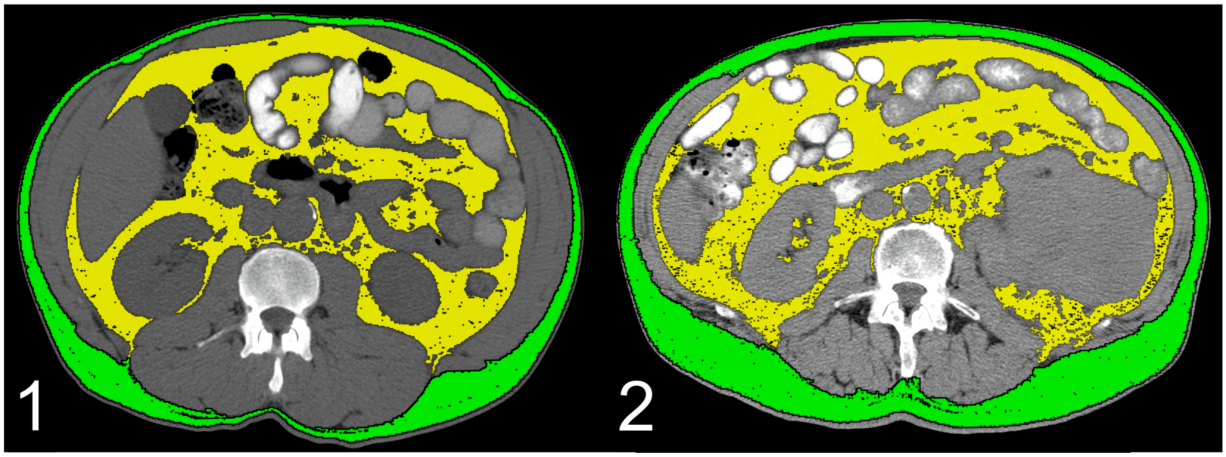

Figure 2. *Representative abdominal adipose tissue segmentation. Axial non-contrast CT images acquired 3 cm superiorly to the inferior endplate of the third lumbar vertebra (L3), showing semi-automated segmentation of abdominal fat compartments performed with Horos v4.0.0 RC2. Adipose tissue was identified within the attenuation range of −190 to −30 HU. The VAT area was delineated using the yellow ROI, corresponding to intra-abdominal fat within the muscular fascia. In contrast, the SAT area was delineated using the green ROI, including the adipose tissue located between the skin and the muscular fascia. TAT was calculated as the sum of VAT and SAT. Panel 1 shows a representative GIMAP-positive case, and panel 2 a representative GIMAP-negative case. Both demonstrate comparable segmentation areas and fat distribution patterns.*

Statistical Analysis

In the traditional statistical analysis, conducted using Student's t-tests without correction for multiple comparisons, no significant differences were observed between the GIMAP-positive and GIMAP-negative groups across the radiological compartments evaluated. Specifically, mean tumor density did not differ significantly between the two groups (p=0.180), nor did minimum and maximum values (p=0.183 and p=0.811, respectively). Similarly, measurements of abdominal adipose tissue areas showed no significant variation: total, visceral, and subcutaneous fat areas were not different between GIMAP-positive and GIMAP-negative patients (p=0.449, p=0.848, p=0.137). Liver parameters were also comparable, with mean, minimum, and maximum density values showing no statistically relevant differences between the groups (p=0.500, p=0.900, p=0.536). Overall, analyses using standard statistical tests reveal no significant associations between GIMAP expression and the radiological characteristics of tumors, adipose tissue, or the liver.

Statistical Analysis with Computational Support

Statistical analyses were performed using established methods, including Welch's t-tests with FDR-BH correction, equivalence testing, effect size estimation (Hedges' g), power analysis, and robust winsorization. Computational support (GPT-5) was employed solely to automate dataset harmonization, variable coding, and script generation. All analyses were reviewed and validated by the research team to ensure methodological accuracy. Artificial Intelligence (AI) was used to harmonize radiological datasets for adipose tissue, liver, and tumor, to code group variables (GIMAP-positive and GIMAP-negative), and to perform an extended statistical analysis workflow. Welch's t-tests were applied with multiple comparison correction using the FDR-BH procedure, effect sizes were estimated through Hedges' g with 95% confidence intervals, and equivalence testing (TOST) was performed with clinically relevant thresholds corresponding to Cohen's d of ±0.3 and ±0.5. Post-hoc power analysis was used to estimate the Minimum Detectable Effect at 80 percent power, and robust testing with 5 percent winsorization was performed to reduce the influence of outliers. The AI also flagged possible inconsistencies in hepatic HU values related to scaling factors in data export, suggesting methodological verification without affecting the statistical comparisons. All results were reviewed and validated by the research team.

Results

Statistical Analysis Results

In the 177 cases of ccRCC analyzed, no statistically significant differences in tumor attenuation values were observed between GIMAP-positive and GIMAP-negative tumors. Specifically, mean tumor attenuation was 36.61 HU in GIMAP-positive cases, compared with 34.61 HU in GIMAP-negative cases (p=0.180; Table 1), with minimum and maximum values comparable between the two groups.

Table 1: Hounsfield Units (HU) on unenhanced computed tomography (CT) scans of clear cell renal cell carcinoma (ccRCC), stratified by GTPase of immunity-associated proteins (GIMAP) expression.

Tumor HU	**Overall**	**Negative GIMAP**	**Positive GIMAP**	**p-value[2]**
	(n = 177)	**(n = 131, 74.07%)**	**(n = 46, 25.93%)**	
Tumor HU mean	35.1[1] (8-60)	34.6[1] (8-60)	36.6[1] (24-52)	0.18
Tumor HU minimum	−8.3[1] (−100-33)	−7.9[1] (−100-33)	−5[1] (−49-24)	0.183
Tumor HU maximum	79.7[1] (42-153)	79.9[1] (42-153)	79.1[1] (51-137)	0.811

[1]Mean
[2]*Student's t-test*
Values in bold indicate statistical significance set at p<0.05

The assessment of abdominal adipose tissue compartments in 194 patients also showed no significant associations with GIMAP expression: TAT averaged 431.1 cm² in GIMAP-positive cases and 407.3 cm² in GIMAP-negative ones (p=0.449), VAT 197.1 vs. 200.8 cm² (p=0.848), and SAT 233.9 vs. 206.4 cm² (p=0.137; Table 2).

Table 2: cross-sectional areas of total adipose tissue (TAT), visceral adipose tissue (VAT), and subcutaneous adipose tissue (SAT) stratified by GTPase of immunity-associated proteins (GIMAP) expression.

Abdominal adipose tissue compartments	**Overall**	**Negative GIMAP**	**Positive GIMAP**	**p-value[2]**
	(n = 194)	**(n = 147, 75.80%)**	**(n = 47, 24.20%)**	
TAT	413[1] (79-914.7)	407.3[1] (87.2-914.7)	431[1] (79-900.9)	0.449
VAT	199.9[1] (10-726)	200.8[1] (15-726)	197.1[1] (10-391)	0.848
SAT	213[1] (59-632)	206.4[1] (59-632)	233.9[1] (62-561)	0.137

[1]Mean
[2]Student's t-test
Values in bold indicate statistical significance set at p<0.05

Similarly, hepatic attenuation parameters, evaluated in 205 patients, did not differ significantly according to GIMAP status: mean hepatic attenuation was 61.1 HU in GIMAP-positive tumors and 59.3 HU in GIMAP-negative tumors (p=0.500), with comparable minimum and maximum values between groups (Table 3).

Table 3: Hounsfield Units (HU) on unenhanced computed tomography (CT) scans of liver, stratified by GTPase of immunity-associated proteins (GIMAP) expression.

Hepatic HU	**Overall**	**Negative GIMAP**	**Positive GIMAP**	**p-value[2]**
	(n = 205)	**(n = 160, 78.05%)**	**(n = 45, 21.95%)**	
Hepatic HU mean	59.7[1] (18-134)	59.3[1] (18-110)	61.1 (29-134)	0.5
Hepatic HU minimum	10.5[1] (−63-81)	10.5[1] (−63-81)	10.6[1] (−48-59)	0.9
Hepatic HU maximum	108.6[1] (54-228)	108[1] (54-193)	110.5[1] (66-228)	0.536

[1]Mean
[2]*Student's t-test*
Values in bold indicate statistical significance set at p<0.05

Overall, the radiogenomic analysis did not reveal statistically significant correlations between GIMAP gene family expression and lipid metabolism imaging features on CT.

AI-Assisted Statistical Analysis

The comparison between GIMAP-positive and GIMAP-negative groups did not reveal statistically significant differences after correction for multiple testing. Effect sizes, expressed as Hedges' g, were generally small, indicating no relevant associations. Equivalence testing showed that, with a threshold corresponding to Cohen's d of ±0.3, equivalence could not be demonstrated. In contrast, with a wider threshold of ±0.5, several adipose, hepatic, and tumor variables met the criteria for equivalence, allowing the exclusion of at least medium-sized effects. Power analysis indicated a Minimum Detectable Effect between 0.45 and 0.48 in terms of Cohen's d, confirming that the study had sufficient sensitivity to exclude medium but not small effects. Robust analyses using winsorized data confirmed the stability of the findings, except for a borderline signal in SAT that did not persist after correction for multiple comparisons. Overall, the application of AI-assisted methods strengthens the interpretation of the study, supporting the absence of clinically relevant differences in the radiological parameters examined between GIMAP-positive and GIMAP-negative patients.

Discussion

In this study, we investigated the association between GIMAP gene family expression and imaging features related to lipid metabolism in patients with ccRCC. Our analysis, based on CT-derived measurements of tumor attenuation, abdominal adipose tissue distribution, and hepatic attenuation, did not reveal statistically significant correlations with GIMAP expression. These findings suggest that, despite the established role of GIMAPs in lymphocyte biology and immune regulation, their expression does not appear to be reflected in radiological markers of lipid content or adipose tissue distribution in ccRCC.

Previous studies have highlighted the potential of radiogenomics to non-invasively capture tumor biology and to predict molecular subtypes of renal cancer. In particular, GIMAP-positive tumors have been associated with aggressive clinicopathological and radiological features, including higher Fuhrman grade and evidence of infiltrative growth [1]. However, our results indicate that this radiogenomic signature does not extend to parameters related to lipid metabolism, such as intracellular lipid accumulation or abdominal adipose tissue compartments.

Beyond the negative findings of our analysis, the present data refine how GIMAP biology should be interpreted in ccRCC radiogenomics. GIMAPs are small GTPases with immune-restricted functions, best known for controlling lymphocyte development, survival, and homeostasis; perturbations in this family alter T-cell fate and peripheral maintenance rather than core metabolic programs of parenchymal tumor cells. This immune-centric role is highlighted by the dependence of T and B lymphocytes on GIMAPs and by the limited direct connection with lipid metabolism pathways [14]. In line with that biology, prior radiogenomic work specifically focused on GIMAPs in ccRCC reported associations with aggressive clinicopathologic and morphologic traits on CT, older age, higher grade, and exophytic/infiltrative features [1]. Our results extend that observation by showing that CT surrogates of lipid metabolism (tumor HU, hepatic HU, and abdominal adipose tissue compartments) are not aligned with GIMAP expression status.

Adipose differentiation-related protein (ADFP), which plays a key role in fatty acid uptake and lipid droplet formation, is markedly overexpressed in ccRCC at both the mRNA and protein levels [21–23]. High levels of ADFP expression are also found in adipocytes [24]. ADFP is a hypoxia-responsive gene whose transcription is regulated by hypoxia-inducible factors (HIFs) [25]. The von Hippel–Lindau protein (VHLp) forms a complex that promotes HIF degradation; however, mutations in VHL inactivate VHLp, preventing HIF degradation and, consequently, triggering pro-angiogenic pathways that support cell proliferation [26–29]. Thus, VHL mutations, by impairing HIF inactivation, may contribute to increased ADFP expression in ccRCC [24]. Moreover, HIFs repress CPT1A, the key enzyme for mitochondrial fatty acid transport. This repression blocks fatty acid oxidation and redirects it into lipid droplets. Lipid droplet formation is promoted under CPT1A suppression. Functionally, low CPT1A is required for tumor growth, while high CPT1A limits it. In human tumors, CPT1A

expression is reduced compared with normal kidney tissue, and lower levels correlate with worse patient outcomes. Thus, HIF-driven control of fatty acid metabolism is essential for ccRCC tumorigenesis [30].

In clinical imaging cohorts, radiogenomic analyses have therefore concentrated on ADFP, showing reproducible links between ADFP status and CT-derived lipid metrics in ccRCC, including lower minimum tumoral HU and hepatic attenuation patterns consistent with lipid overload [4,5]. Together, these data help explain why GIMAPs, a family tied to lymphocyte biology, do not map onto CT lipid surrogates, whereas metabolic regulators such as ADFP do.

In ccRCC computational oncology analyses have linked GIMAP expression with immune infiltration signatures and overall survival, reinforcing the notion that GIMAPs capture immune rather than metabolic dimensions of tumor biology [31]. Our findings are consistent with this separation: CT features keyed to lipid metabolism fail to mirror GIMAP status, whereas GIMAP-related signals may be better explored alongside TIME metrics (e.g., T-cell density, neutrophil-to-lymphocyte radiomics, or perfusion/necrosis patterns tied to inflamed phenotypes).

An additional layer is the interaction between adipose tissue and kidney cancer risk and outcomes. Multiple imaging-based epidemiologic studies have implicated abdominal fat, especially VAT, in the presentation and prognosis of ccRCC, although results vary by cohort and endpoint.

For example, a study retrospectively analyzed 250 patients with ccRCC, divided into two groups based on T stage: 173 with low T stage and 77 with high T stage [32].

Using preoperative CT images, the researchers measured subcutaneous fat area, visceral fat area (VFA), and total fat area (TFA), and calculated the relative visceral fat area:

$$rVFA = VFA/TFA.$$

They also evaluated blood-based indicators related to nutrition and inflammation.

The most notable findings emerged in the low T-stage group. Patients who experienced short-term postoperative complications had a significantly lower rVFA compared with those without complications. In contrast, no statistically significant association was observed in the high T-stage group.

Furthermore, correlations between blood-based nutritional/inflammatory parameters and fat-related variables differed between the two T-stage groups, suggesting that the interaction between systemic biomarkers and adipose tissue characteristics may vary by tumor stage.

The authors concluded that rVFA is an independent and reliable predictor of short-term prognosis in patients with ccRCC at low T stage, but not in those with high T stage [32].

Another study investigated whether VAT, measured on preoperative CT scans, can help predict recurrence-free survival in patients with localized ccRCC [33]. Researchers analyzed data from 446 patients who underwent curative surgery.

The analysis revealed a U-shaped relationship between rVFA and recurrence-free survival. Patients with very low or especially high rVFA values had worse outcomes, with a clear risk increase when rVFA exceeded 0.40. Using advanced statistical and machine learning approaches, including random survival forest models, rVFA consistently emerged as one of the strongest predictors of recurrence risk. The predictive model achieved high accuracy, particularly for short- to mid-term outcomes.

We found that rVFA is a practical and valuable prognostic biomarker in localized ccRCC. Since it can be easily measured with routine CT imaging, it may help clinicians better stratify patients by risk of recurrence after surgery [33]. Clinically, these insights carry two implications. First, CT-based lipid features are unlikely to serve as surrogates for GIMAP status, so attempting to infer immune-gene expression from HU or adipose compartment areas may be misguided. Second, multi-parametric models that partition immune and metabolic axes —for example, combining radiomics of tumor architecture/necrosis (immune-linked) with attenuation/radiodensity measures (metabolic-linked) —and integrating them with genomics or transcriptomics, may yield more accurate phenotyping and risk stratification in ccRCC.

However, several limitations merit emphasis. Retrospective design and reliance on TCIA introduce variability in scanners, protocols, and ROI placement, potentially diluting subtle relationships between immune genes and imaging phenotypes. Our lipid metrics (unenhanced HU

and single-slice adiposity measures) are pragmatic surrogates but may not fully capture the spatial heterogeneity of lipid composition. Moreover, we did not quantify TIME features (e.g., CD8 density, tertiary lymphoid structures) that could co-vary with GIMAP status; future work should integrate such endpoints to test whether immune radiomic markers, rather than lipid markers, align with GIMAPs. Finally, the lack of an external validation cohort prevents us from confirming the robustness of our observations across independent datasets, underscoring the need for prospective multicenter studies to validate and extend these results. This immunometabolic crosstalk offers a plausible route by which adiposity could influence antitumor immunity in ccRCC. However, and critically for interpreting our imaging results, this pathway does not imply that GIMAP expression in tumors should correlate with CT surrogates of lipid storage. Rather, any influence of adiposity on GIMAP-related immunity is more likely to appear through immune infiltration/activation signatures than through HU-based lipid metrics.

Conclusion

In summary, our study shows that GIMAP expression tracks the immune axis of ccRCC, whereas CT lipid surrogates primarily reflect HIF-driven metabolic reprogramming, as captured by ADFP-related pathways. The absence of an association between GIMAP status and HU-based lipid features is therefore biologically coherent. It guides future radiogenomic modeling toward multi-axis integration rather than single-marker surrogacy.

Authors' Contributions

Conceptualization, F.G. and C.A.M.; methodology, F.G., A.P, A.T., and C.A.M.; software, F.G., M.C., and C.A.M.; validation, F.G. and C.A.M.; formal analysis, F.G. and C.A.M.; investigation, F.G. and C.A.M.; resources, F.G. and C.A.M.; data curation, F.G. and C.A.M.; writing – original draft preparation, F.G. and C.A.M.; writing, review, and editing, F.G. and C.A.M.; visualization, F.G. and C.A.M.; supervision, F.G., B.B.Z., and C.A.M.; project administration, F.G. and C.A.M. All authors have read and agreed to the published version of the manuscript.

Funding: No external funding was used to realize this work.

Acknowledgments: N/A

Conflicts of Interest: The authors declare no conflict of interest. For a statement, please write to the journal office at editor@precisionnanomedicine.com.

Quote this article as Federico Greco, Cataldo M., Panunzio A., Tafuri A., Zobel BB., Mallio CA, GIMAP and Lipid Metabolism Imaging in Clear Cell Renal Cell Carcinoma: A Negative Radiogenomic Analysis, Precis. Nanomed. 2025,8(4):1600-1610 https://doi.org/10.33218/001c.145452.

REFERENCES

1. Greco F, Panunzio A, Tafuri A, Bernetti C, Pagliarulo V, Beomonte Zobel B, et al. Radiogenomic Features of GIMAP Family Genes in Clear Cell Renal Cell Carcinoma: An Observational Study on CT Images. Genes. 2023;14:1832.

2. Greco F, Cataldo M, Beomonte Zobel B, Mallio CA. Failure to Suppress Progression in Clear Cell Renal Cell Carcinoma Associated with NCOA7 Low Expression Revealed Through Radiogenomic Analysis. Genes. 2025;16:386.

3. Greco F, Panunzio A, Bernetti C, Tafuri A, Beomonte Zobel B, Mallio CA. The Radiogenomic Landscape of Clear Cell Renal Cell Carcinoma: Insights into Lipid Metabolism through Evaluation of ADFP Expression. Diagnostics. 2024;14:1667.

4. Greco F, Panunzio A, D'Andrea V, Vescovo M, Tafuri A, Carotti S, et al. Exploring Tumor Heterogeneity: Radiogenomic Assessment of ADFP in Low WHO/ISUP Grade Clear Cell Renal Cell Carcinoma. Cancers. 2024;16:3164.

5. Greco F, Panunzio A, Cerroni L, Cea L, Bernetti C, Tafuri A, et al. CT Characterization of Lipid Metabolism in Clear Cell Renal Cell Carcinoma: Relationship Between Liver Hounsfield Unit Values and Adipose Differentiation-Related Protein Gene Expression. Int J Mol Sci. 2024;25:12587.
6. Pagès F, Kirilovsky A, Mlecnik B, Asslaber M, Tosolini M, Bindea G, et al. In situ cytotoxic and memory T cells predict outcome in patients with early-stage colorectal cancer. J Clin Oncol. 2009;27:5944–51.
7. Gajewski TF, Schreiber H, Fu YX. Innate and adaptive immune cells in the tumor microenvironment. Nat Immunol. 2013;14:1014–22.
8. Tumeh PC, Harview CL, Yearley JH, Shintaku IP, Taylor EJ, Robert L, et al. PD-1 blockade induces responses by inhibiting adaptive immune resistance. Nature. 2014;515:568–71.
9. Krucken J, Schroetel RM, Muller IU, Saidani N, Marinovski P, Benten WP, et al. Comparative analysis of the human gimap gene cluster encoding a novel GTPase family. Gene. 2004;341:291–304.
10. Zenz T, Roessner A, Thomas A, Frohling S, Dohner H, Calabretta B, et al. hIan5: the human ortholog to the rat Ian4/Iddm1/lyp is a new member of the Ian family that is overexpressed in B-cell lymphoid malignancies. Genes Immun. 2004;5:109–16.
11. Datta P, Webb LM, Avdo I, Pascall J, Butcher GW. Survival of mature T cells in the periphery is intrinsically dependent on GIMAP1 in mice. Eur J Immunol. 2017;47:84–93.
12. Webb LM, Datta P, Bell SE, Kitamura D, Turner M, Butcher GW. GIMAP1 Is Essential for the Survival of Naive and Activated B Cells In Vivo. J Immunol. 2016;196:207–16.
13. Limoges MA, Cloutier M, Nandi M, Ilangumaran S, Ramanathan S. The GIMAP Family Proteins: An Incomplete Puzzle. Front Immunol. 2021;12:679739.
14. Schnell S, Demolliere C, van den Berk P, Jacobs H. Gimap4 accelerates T-cell death. Blood. 2006;108:591–9.
15. Ho CH, Tsai SF. Functional and biochemical characterization of a T cell-associated anti-apoptotic protein, GIMAP6. J Biol Chem. 2017;292:9305–19.
16. Gao F, Litchfield B, Wu H. Adipose tissue lymphocytes and obesity. J Cardiovasc Aging. 2024;4:5.
17.de Cubas AA, Rathmell WK. Epigenetic modifiers: Activities in renal cell carcinoma. Nat Rev Urol. 2018;15:599–614.
18. Fischer-Posovszky P, Wabitsch M, Hochberg Z. Endocrinology of adipose tissue—An update. Horm Metab Res. 2007;39:314–21.
19. Raucci R, Rusolo F, Sharma A, Colonna G, Castello G, Costantini S. Functional and structural features of adipokine family. Cytokine. 2013;61:1–14.
20. CIP TCGA Radiology Initiative—The Cancer Imaging Archive (TCIA) Public Access—Cancer Imaging Archive Wiki [Internet]. https://wiki.cancerimagingarchive.net/display/Public/CIP+TCGA+Radiology+Initiative. Accessed 01 Nov 2019.
21. Jiang HP, Serrero G. Isolation and characterization of a full-length cDNA coding for an adipose differentiation-related protein. Proc Natl Acad Sci USA. 1992;89:7856–60.
22. Londos C, Brasaemle DL, Schultz CJ, Segrest JP, Kimmel AR. Perilipins, ADRP, and other proteins that associate with intracellular neutral lipid droplets in animal cells. Semin Cell Dev Biol. 1999;10:51–8.
23. Yao M, Tabuchi H, Nagashima Y, Baba M, Nakaigawa N, Ishiguro H, et al. Gene expression analysis of renal carcinoma: Adipose differentiation-related protein as a potential diagnostic and prognostic biomarker for clear-cell renal carcinoma. J Pathol. 2005;205:377–87.
24. Brasaemle DL, Barber T, Wolins NE, Serrero G, Blanchette-Mackie EJ, Londos C. Adipose differentiation-related protein is an ubiquitously expressed lipid storage droplet-associated protein. J Lipid Res. 1997;38:2249–63.
25. Saarikoski ST, Rivera SP, Hankinson O. Mitogen-inducible gene 6 (MIG-6), adipophilin, and tuftelin are inducible by hypoxia. FEBS Lett. 2002;530:186–90.
26. Brugarolas J. Molecular genetics of clear-cell renal cell carcinoma. J Clin Oncol. 2014;32:1968–76.
27. Stebbins CE, Kaelin WG Jr, Pavletich NP. Structure of the VHL-ElonginC–ElonginB complex: Implications for VHL tumor suppressor function. Science. 1999;284:455–61.

28. Maxwell PH, Wiesener MS, Chang GW, Clifford SC, Vaux EC, Cockman ME, et al. The tumor suppressor protein VHL targets hypoxia-inducible factors for oxygen-dependent proteolysis. Nature. 1999;399:271–5.
29. Kase AM, George DJ, Ramalingam S. Clear Cell Renal Cell Carcinoma: From Biology to Treatment. Cancers. 2023;15:665.
30. Du W, Zhang L, Brett-Morris A, Aguila B, Kerner J, Hoppel CL, et al. HIF drives lipid deposition and cancer in ccRCC via repression of fatty acid metabolism. Nat Commun. 2017;8:1769.
31. Zhang M, Zhang X, Hou J, Liang X, Zhang M. Prognostic and Immune Infiltration Signatures of GIMAP Family Genes in Clear Cell Renal Cell Carcinoma. Front Biosci (Landmark Ed). 2023;28:308.
32. Guo H, Zhang Y, Ma H, Gong P, Shi Y, Zhao W, et al. T-stage-specific abdominal visceral fat, haematological nutrition indicators and inflammation as prognostic factors in patients with clear renal cell carcinoma. Adipocyte. 2022;11:133–42.
33. Feng Z, Wu Y, Hu Z, Yang P, Li Z. Visceral fat measured with CT helps predict recurrence-free survival in patients with localized clear cell renal cell carcinoma. Int Urol Nephrol. 2025.
34. Gao F, Litchfield B, Wu H. Adipose tissue lymphocytes and obesity. J Cardiovasc Aging. 2024;4:5.